

Effects of colloid polydispersity on the phase behaviour of colloid-polymer mixtures

Moreno Fasolo and Peter Sollich

Department of Mathematics, King's College London, Strand, London WC2R 2LS, UK

(Dated: November 21, 2018)

We study theoretically the equilibrium phase behaviour of a mixture of *polydisperse* hard-sphere colloids and monodisperse polymers, modelled using the Asakura-Oosawa model within the free volume approximation of Lekkerkerker *et al.* We compute full phase diagrams in the plane of colloid and polymer volume fractions, using the moment free energy method. The intricate features of phase separation in pure polydisperse colloids combine with the appearance of polymer-induced gas-liquid coexistence to give a rich variety of phase diagram topologies as the polymer-colloid size ratio ξ and the colloid polydispersity δ are varied. Quantitatively, we find that polydispersity disfavours fluid-solid against gas-liquid separation, causing a substantial *lowering* of the threshold value ξ_c above which stable two-phase gas-liquid coexistence appears. Phase splits involving two or more solids can occur already at low colloid concentration, where they may be kinetically accessible. We also analyse the strength of colloidal size fractionation. When a solid phase separates from a fluid, its polydispersity is reduced most strongly if the phase separation takes place at low colloid concentration and high polymer concentration, in agreement with experimental observations. For fractionation in gas-liquid coexistence we likewise find good agreement with experiment, as well as with perturbative theories for near-monodisperse systems.

PACS numbers: 64.70Fx, 68.35.Rh

I. INTRODUCTION

Since the 1980s phase separation phenomena in colloidal suspensions that are induced by the addition of polymers have gradually gained interest both from a technological and scientific point of view. The equilibrium phase behaviour of a pure colloidal hard sphere system is dictated exclusively by entropic effects, and these can cause separation into fluid and solid phases. The term fluid is used to emphasise that there are no separate gas and liquid phases in such a system. However, such phases can appear with the addition of polymer, because of the effective colloid-colloid attraction which this induces. Our aim in this paper is to study the effect in which colloid *polydispersity*, i.e. a continuous spread of colloid sizes, further affects the phase behaviour. Because polydispersity causes complex phase equilibria even for pure hard spheres [1, 2], with for example the coexistence of a fluid with several solids, one expects very rich phase behaviour when polymer is added.

A theoretical model of phase separation in a mixture of colloidal and polymer particles was first advanced by Asakura and Oosawa (AO) [3] and extended by Vrij [4]. In order to describe the interactions in a solution with *non-adsorbing* polymers, they proposed to model each polymer chain as a sphere with diameter σ_p equal to twice the radius of gyration. These “polymer spheres” are then assumed to be able to interpenetrate freely with each other, which is a reasonable assumption for polymers near their θ -point where the chains obey random walk statistics. On the other hand, the polymer chains are completely excluded from the space occupied by the colloidal particles, corresponding to a hard interaction between polymers and colloids.

Overall, the AO model is effectively a mixture of hard spheres, but with extreme non-additivity in the polymer-

polymer interaction which has range zero rather than σ_p . Explicitly, the AO interparticle potentials can be expressed as follows:

$$v_{cc}(r) = \begin{cases} \infty & \text{if } r < \frac{1}{2}(\sigma_c + \sigma'_c) \\ 0 & \text{otherwise} \end{cases} ;$$

$$v_{cp}(r) = \begin{cases} \infty & \text{if } r < \frac{1}{2}(\sigma_c + \sigma_p) \\ 0 & \text{otherwise} \end{cases} ; \quad v_{pp}(r) = 0$$

Here r is the distance between the centres of mass of the particles considered. The subscript “cc” refers to an interaction between two colloidal particles; in a polydisperse system these can have different diameters σ_c and σ'_c . Similarly “cp” and “pp” denote colloid-polymer and polymer-polymer interactions, respectively.

Even though all the interactions are still hard within this model, the entropy of the polymers induces an effective attraction between the colloids. The centres of mass of the polymers are excluded from a spherical “exclusion zone” of width $\sigma_p/2$ around the colloids. When the exclusion zones of two or more colloids overlap, the polymers cannot access the region between the colloids. The osmotic pressure of the polymers is then unbalanced and creates an attractive *depletion interaction* between the colloids. Its range is set by the polymer diameter σ_p , and its strength at contact is found to be proportional to $\sigma_p^2 \sigma_c$ times the osmotic pressure of the polymers. It is this depletion interaction which can cause the suspension to separate into colloid-poor and colloid-rich phases, resulting in phase equilibria with solid, liquid or gas phases depending on conditions. These striking effects have been extensively investigated experimentally [5–9] and the AO model has been shown to give a good description for suspensions of sterically stabilised colloidal particles immersed in a solvent with polymers [10, 11]. However, experimental systems are always polydisperse, containing a spread of colloid sizes as well as polymer chain lengths.

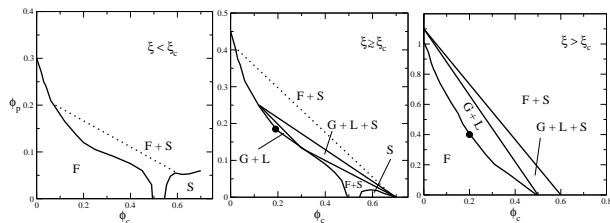


FIG. 1: Phase diagram sketch for colloid-polymer mixtures with three different values of the size ratio ξ . For $\xi < \xi_c$ the depletion interaction is weak and the only effect is the widening of the (F)luid-(S)olid coexistence region; at $\xi > \xi_c$ (right) the longer polymers create a sufficiently long-range interaction that induces the formation of (G)as and (L)iquid phases and hence of a critical point, marked with a circle. The crossover value $\xi \approx \xi_c$ (middle) is the value where a region of gas-liquid coexistence first appears.

As reviewed below, our theoretical understanding of the effects of this polydispersity on the phase behaviour remains very limited. Ideally, one would therefore like to be able to study theoretically the phase behaviour of a mixture of colloids and polymers that are both polydisperse. This is a very challenging problem. As a first step we therefore focus in this paper on the case where *only* the colloids are treated as polydisperse. This already turns out to result in very rich phase behaviour.

We first review some of the previous work carried out on colloid-polymer mixtures. Most theoretical studies have focused on the case where the colloids are monodisperse and the polymers are either monodisperse or polydisperse. Theoretical work by Gast *et al* [12], Lekkerkerker *et al* [10] and Dijkstra *et al* [11] for a monodisperse mixture predicts that the topology of the phase diagram depends crucially on the range σ_p of the depletion interaction, or more precisely the ratio $\xi = \sigma_p/\sigma_c$ of the polymer and colloid diameters. This is sketched in Fig. 1, which shows phase diagrams in terms of colloid volume fraction ϕ_c and effective polymer volume fraction ϕ_p . The latter is defined as the polymer concentration ρ_p times the volume $(\pi/6)\sigma_p^3$ of each polymer and can be greater than 1 because the polymers can overlap.

To understand these phase diagrams, one can imagine gradually adding polymers to a pure (monodisperse) colloidal hard-sphere system which exhibits coexistence between a fluid and a crystalline solid with volume fractions of around 50% and 55%, respectively [13–15]. For size ratios ξ below a certain crossover value ξ_c the addition of polymer only has the effect of widening the fluid-solid coexistence region; see Fig. 1 (left). This widening is gradual at first but then becomes very pronounced. It has been argued that, when viewed in terms of the colloid system with its effective polymer-induced attraction, this can be understood as the crossover from a regime with dominant entropic effects to an “energetic fluid” regime where the strength at contact of the attractive interaction is the key parameter [16].

For sufficiently large polymers, on the other hand ($\xi > \xi_c$), the addition of polymeric particles leads to a new phase diagram topology where gas-liquid (and therefore gas-liquid-solid) coexistence can occur, as shown in Fig. 1 (right). The threshold value ξ_c of the size ratio is the one where a gas-liquid region first appears; see Fig. 1 (middle). The intuitive explanation for the different behaviour at small and large ξ is that if the interaction is generated by sufficiently long polymers, $\xi > \xi_c$, then neighbouring colloids can still be within the range of the attraction even when they are in a disordered state, and so a thermodynamically stable liquid phase can form.

The actual crossover value ξ_c varies slightly depending on the theory considered but is found to lie in the range $\xi_c \approx 0.3 \dots 0.6$. E.g. in [11] a colloid system with the effective AO interaction was simulated with the result $0.4 < \xi_c < 0.6$; this result is approximate because in this range of ξ the effective interaction potential for the colloids also contains many-body terms. Lekkerkerker *et al* [10], by the use of a van der Waals-type approximation (see below) identified $\xi_c \approx 0.32$, and Gast and collaborators [12], with the aid of perturbation theory, estimated ξ_c to be $\approx 1/3$. On the experimental side Ilett *et al* [5] found instead $\xi_c \approx 0.25$ for a suspension with polydispersity δ of order 0.05. One of the goals of our study will be to identify the effects of colloidal polydispersity on the threshold value ξ_c .

Initial attempts to understand the influence of polydispersity on colloidal-polymer mixtures have been made in recent years, but with a focus on size-polydispersity in the *polymers* [17–20] which causes quantitative rather than qualitative changes in the phase diagrams. To the best of our knowledge the only studies considering polydisperse *colloids* investigate the liquid-gas phase separation in the limit of near-monodisperse colloids, where perturbative theories can be applied [9, 21, 22]. In this regime it turns out that the gas-liquid coexistence region widens as the colloidal spheres becomes more polydisperse [22]. This statement applies when the osmotic pressure of the polymer – or equivalently its chemical potential – is imposed, e.g. by connecting the colloid-polymer mixture to a large polymer reservoir. This corresponds to fixing the effective interaction between the colloids. More recent experimental work [9] has focused on the strength of size fractionation between coexisting phases and its scaling with the overall colloid polydispersity; we return to a comparison with this study in Sec. VB.

We provide here a theoretical analysis of phase equilibria in colloid-polymer mixtures with significant size-polydispersity in the colloids. The paper is structured as follows. In Sec. II we derive the free energy of the polydisperse AO model, within the free volume approximation employed by Lekkerkerker *et al* [10]. This free energy has a truncatable [23] structure, allowing us to solve the resulting phase equilibrium equations by using the moment free energy (MFE) method as explained in Sec. III. In Sec. IV we study the phase diagram topologies that arise, while Sec. V is devoted to a quantitative

analysis of the effects of polydispersity and polymer size on the phase diagrams, and of colloidal size fractionation between coexisting phases. Conclusions and an outlook towards future work are given in Sec. VI.

II. FREE VOLUME THEORY

Even though in the AO model the polymer-polymer interactions are ideal, a direct calculation of the partition function is a difficult task because one needs to keep track of the overlaps of all exclusion zones around the colloids; the remaining free volume accessible to the polymers thus depends in a complicated way on the configuration of the colloids. Even if only pairwise overlaps are considered one still effectively has a colloid system with a depletion interaction potential of finite range, which cannot be solved exactly. Progress can however be made by using a van der Waals or free volume approximation which replaces the free volume by its average over colloid configurations. This will lead us to an explicit expression for the Helmholtz free energy of our system as a sum of two contributions, one corresponding to the pure hard-sphere system and one describing the average interaction between polymers and colloids.

In what follows we will derive the free volume approximation to the free energy for a system where both the polymers and colloids are polydisperse. Allowing for polydispersity in the polymers adds almost no extra work and facilitates comparison with other approaches. The case of monodisperse polymers which we later study numerically is easily recovered as a special case.

We assume initially that we have a discrete mixture of colloid and polymer species and take the polydisperse limit at the end. The colloid species are labelled by s , with $\{N_{cs}\}$ the number of particles of each species and σ_{cs} their diameter; similarly $\{N_{pt}\}$ and σ_{pt} give the number of particles and diameter for each of the polymer species. Because all interactions in the AO model are hard, temperature becomes an irrelevant scale factor which only sets the energy scale. We therefore measure all energies in units of $T = 1/\beta$ and set k_B to one. The spatial coordinates of the particles are denoted by R_i for the colloids and r_j for the polymers. The canonical partition function is then

$$Z = \prod_{s,t} \frac{\lambda_{cs}^{-3N_{cs}} \lambda_{pt}^{-3N_{pt}}}{N_{cs}! N_{pt}!} \int dR dr \times \exp \left[- \sum_{i < i'} v_{cc}(i, i') - \sum_{i,j} v_{cp}(i, j) \right] \quad (1)$$

where $v_{cc}(i, i')$ stands for $v_{cc}(|R_i - R_{i'}|)$ and similarly for $v_{cp}(i, j)$. The integrations dR, dr extend over all colloid and polymer coordinates, and λ_{cs} and λ_{pt} are the de Broglie wavelengths for each species. The natural thermodynamic potential to work with, in this context, is the semi-grand canonical potential. For this the system can

be thought of as connected to a polymer reservoir via a membrane impermeable to colloids but permeable to polymers, so that the polymer particle numbers $\{N_{pt}\}$ can range over all possible values. The resulting semi-grand partition function is given by

$$\Xi(\{N_{cs}\}, V, \{\mu_{pt}\}) = \sum_{\{N_{pt}\}} \prod_t e^{\mu_{pt} N_{pt}} Z(\{N_{cs}\}, \{N_{pt}\}, V) \quad (2)$$

where the chemical potentials μ_{pt} of the polymers are fixed by the reservoir. In (2) we can separate the ideal contributions from the excess part:

$$\Xi = Z_{\text{hs}}^0 \sum_{\{N_{pt}\}} \int \frac{dR}{V^{N_c}} \exp \left(- \sum_{i < i'} v_{cc}(i, i') \right) \times \prod_t \frac{V^{N_{pt}}}{N_{pt}!} \left(\int \frac{dr_{j(t)}}{V} \frac{e^{\mu_{pt}}}{\lambda_{pt}^3} e^{-\sum_{i,j} v_{cp}(i,j)} \right)^{N_{pt}} \quad (3)$$

where Z_{hs}^0 is the canonical partition function of an ideal mixture of colloids, $Z_{\text{hs}}^0 = V^{N_c} \prod_s \lambda_{cs}^{-3N_{cs}} / N_{cs}!$ and N_c is the total number of colloids. The quantity $e^{\mu_{pt}} / \lambda_{pt}^3$ identifies the thermodynamic *activity* of the polymer species t , which for our ideal polymers is just its density ρ_{pt}^r in the reservoir. The integration over $r_{j(t)}$, which represents the position of any one of the polymers from species t , gives the fraction of volume available to a hard sphere of diameter σ_{pt} if the colloids are in a configuration $\{R_i\}$, $\alpha(\{R_i\}, \sigma_{pt}) = V^{-1} \int dr_{j(t)} e^{-\sum_i v_{cp}(|R_i - r_j|)}$. We are thus left with a configurational integral over the hard spheres:

$$\Xi = Z_{\text{hs}}^0 \int \frac{dR}{V^{N_c}} \exp \left(- \sum_{i < i'} v_{cc}(i, i') \right) \times \exp \left(V \sum_t \rho_{pt}^r \alpha(\{R_i\}, \sigma_{pt}) \right). \quad (4)$$

Following Widom [24] this can be reinterpreted as an average $\langle \rangle_{\text{hs}}$ over the Boltzmann distribution of the pure colloidal hard-sphere system, with excess partition function $Z_{\text{hs}}^{\text{ex}}$:

$$\Xi = Z_{\text{hs}}^0 Z_{\text{hs}}^{\text{ex}} \left\langle \exp \left(V \sum_t \rho_{pt}^r \alpha(\{R_i\}, \sigma_{pt}) \right) \right\rangle_{\text{hs}} \quad (5)$$

We note that the second exponential in (4) is the effective colloid-colloid interaction generated by the polymers. Beyond trivial zero- and one-body terms it always contains a two-body contribution which is the attractive depletion interaction described above. For sufficiently large polymers ($\xi > 0.154$) also interactions between three or more colloids appear because more than two exclusion zones can overlap simultaneously.

The average in (5) cannot be evaluated exactly. To make progress, we follow the van der Waals approach or

“free volume theory” of Lekkerkerker *et al* [10]. This consists of “moving” the average $\langle \rangle_{\text{hs}}$ inside the exponential to give

$$\Xi = Z_{\text{hs}}^0 Z_{\text{hs}}^{\text{ex}} \exp \left(V \sum_t \rho_{\text{pt}}^r \langle \alpha(\{R_i\}, \sigma_{\text{pt}}) \rangle_{\text{hs}} \right). \quad (6)$$

This approximation is exact in the limit of small polymer activities $\rho_{\text{pt}}^r \rightarrow 0$; otherwise it can be viewed as identifying a lower bound on Ξ , or an upper bound on the thermodynamic potential $\Omega = -\ln \Xi$. The latter becomes

$$\Omega = F_{\text{hs}} - V \sum_t \rho_{\text{pt}}^r \langle \alpha(\{R_i\}, \sigma_{\text{pt}}) \rangle_{\text{hs}} \quad (7)$$

where F_{hs} is the Helmholtz free energy of the pure colloid system. The average free volume $\langle \alpha(\{R_i\}, \sigma_{\text{pt}}) \rangle_{\text{hs}}$ which appears here is the probability of being able to insert a hard particle of diameter σ_{pt} into the pure colloid system. But from the Widom insertion principle [24] this is just $\exp[-\mu_{\text{hs}}^{\text{ex}}(\sigma_{\text{pt}})]$ where $\mu_{\text{hs}}^{\text{ex}}(\sigma)$ is the excess chemical potential of a *colloid* particle of diameter σ , in a system without polymer. The semi-grand potential per unit volume, $\omega = \Omega/V$, can thus be written as

$$\omega = f_{\text{hs}} - \sum_t \rho_{\text{pt}}^r e^{-\mu_{\text{hs}}^{\text{ex}}(\sigma_{\text{pt}})} \quad (8)$$

In the polydisperse limit, the ρ_{pt}^r turn into a reservoir polymer density distribution $\rho_{\text{p}}^r(\sigma_{\text{p}})$ and the sum over t into an integral over σ_{p} so that

$$\omega = f_{\text{hs}} - \int d\sigma_{\text{p}} \rho_{\text{p}}^r(\sigma_{\text{p}}) e^{-\mu_{\text{hs}}^{\text{ex}}(\sigma_{\text{p}})} \quad (9)$$

We note that a similar expression was derived in [20] for the case of monodisperse colloids. This approach used fundamental measure theory and leads to the scaled particle-theory expressions for f_{hs} and $\mu_{\text{hs}}^{\text{ex}}(\sigma)$. Only colloidal gas-liquid demixing was investigated, and the polymer polydispersity was interpreted as arising from the compressibility of polymer chains of a given length. A semi-grand approach, with the slight modification of keeping the total polymer number fixed, is then appropriate because the different polymer “species” can effectively be transformed into each other.

For genuine polymer chain length polydispersity, however, we are in practice dealing with a sample containing a fixed number of polymers of each species. We therefore need to transform back to the canonical ensemble to obtain the Helmholtz free energy density, $f = \omega + \sum_t \mu_{\text{pt}} \rho_{\text{pt}}$. From (8) and bearing in mind the definition of ρ_{pt}^r , the polymer densities and chemical potentials are related by the following transformation:

$$\rho_{\text{pt}} = -\frac{\partial \omega}{\partial \mu_{\text{pt}}} = \lambda_{\text{pt}}^{-3} e^{\mu_{\text{pt}}} e^{-\mu_{\text{c}}^{\text{ex}}(\sigma_{\text{pt}})} = \rho_{\text{pt}}^r e^{-\mu_{\text{c}}^{\text{ex}}(\sigma_{\text{pt}})} \quad (10)$$

Simple algebra then gives for the free energy density

$$f = f_{\text{hs}} + \sum_t \rho_{\text{pt}} (\ln \rho_{\text{pt}} - 1) + \sum_t \rho_{\text{pt}} \mu_{\text{c}}^{\text{ex}}(\sigma_{\text{pt}}) \quad (11)$$

Here we have separated off the ideal polymer part in the second term, dropping the contribution $\sum_t \rho_{\text{pt}} \ln \lambda_{\text{pt}}^3$ which is linear in the densities and therefore leaves the phase behaviour unaffected. In the limit of fully polydisperse polymers the free energy (density) would then read

$$f = f_{\text{hs}} + \int d\sigma_{\text{p}} \rho_{\text{p}}(\sigma_{\text{p}}) [\ln \rho_{\text{p}}(\sigma_{\text{p}}) - 1] + \int d\sigma_{\text{p}} \rho_{\text{p}}(\sigma_{\text{p}}) \mu_{\text{hs}}^{\text{ex}}(\sigma_{\text{p}}) \quad (12)$$

However, in the present study we neglect polydispersity of the polymers and focus on the effects of colloid polydispersity. After separating the free energy f_{hs} of the pure colloid system into its ideal and excess parts, the total free energy (11) then simplifies to $f = f^{\text{id}} + f^{\text{ex}}$, with

$$f^{\text{id}} = \int d\sigma_{\text{c}} \rho_{\text{c}}(\sigma_{\text{c}}) [\ln \rho_{\text{c}}(\sigma_{\text{c}}) - 1] + \rho_{\text{p}} (\ln \rho_{\text{p}} - 1) \\ f^{\text{ex}} = f_{\text{hs}}^{\text{ex}} + \rho_{\text{p}} \mu_{\text{hs}}^{\text{ex}}(\sigma_{\text{p}}). \quad (13)$$

Importantly, evaluation of the free energy (13) requires as nontrivial input only the properties of the pure colloid system, i.e. its excess free energy $f_{\text{hs}}^{\text{ex}}$ and the excess chemical potentials $\mu_{\text{hs}}^{\text{ex}}(\sigma)$ which are obtained by differentiation, $\mu_{\text{hs}}^{\text{ex}}(\sigma) = \delta f_{\text{hs}}^{\text{ex}} / \delta \rho_{\text{c}}(\sigma)$. To specify the free energy fully, we therefore only need to assign appropriate expressions for $f_{\text{hs}}^{\text{ex}}$ in the colloidal fluid (or gas/liquid) and solid phases. For the *fluid* part of the excess free energy the most accurate approximation available is the generalisation by Salacuse and Stell [25] of the BMCSL equation of state [26, 27] while for the *solid* we adopt Bartlett’s fit to simulation data for bidisperse hard sphere mixtures [28, 29]. Our previous work [1, 2] on polydisperse hard spheres has shown that with these free energy expressions quantitatively accurate fits to simulation data are obtained, and so we continue to use them for the present study.

Some care is needed in the application of the excess free energy expression for the solid. The simulation data from which this is derived were obtained for mixtures of two species of hard spheres with diameters differing by no more than $\approx 15\%$. The resulting excess chemical potentials $\mu_{\text{c}}^{\text{ex}}(\sigma)$ are therefore accurate only within a small range around the mean colloid diameter. Outside this range they are unreliable; for example the limiting behaviour predicted from the Widom insertion principle for $\sigma \rightarrow 0$ is not retrieved correctly. This causes a difficulty because in the colloid-polymer interaction term in the free energy (13) we need the excess chemical potential evaluated at the *polymer* diameter, which we will take to be rather smaller than the mean colloid diameter. In fact, it is only in this regime of size ratios ξ well below unity that the AO-model approximation of treating polymers as spherical particles is reasonable; for larger polymers the colloids can “see” the polymer chain structure [30].

To circumvent this problem, we follow previous work within the free volume approach [10, 17, 18] and always

evaluate the excess chemical potential $\mu_c^{\text{ex}}(\sigma_p)$ governing the polymer-colloid interaction from the BMCSL free energy. The underlying physical approximation is that the free volume available to the polymers is not drastically different for colloidal fluid and solid phases so that the *fluid* (BMCSL) expression can also be used to estimate the free volume in colloidal *solids*.

III. MOMENT FREE ENERGY METHOD

A key feature of the excess free energies which we use to describe the colloidal fluid and solid phases is that they are *truncatable* [23]: they depend only on the finite set of moments $\rho_i = \int d\sigma_c \rho_c(\sigma_c) \sigma_c^i$ ($i = 0, \dots, 3$) of the colloidal density distribution $\rho_c(\sigma_c)$. Here $\rho_c(\sigma_c) d\sigma_c$ is the number density of colloids with diameters in the range $\sigma_c \dots \sigma_c + d\sigma_c$. The excess chemical potentials are then third order polynomials,

$$\mu_{\text{hs}}^{\text{ex}}(\sigma) = \frac{\delta f_{\text{hs}}^{\text{ex}}}{\delta \rho_c(\sigma)} = \sum_{i=0}^3 \mu_{\text{hs},i}^{\text{ex}} \sigma^i \quad (14)$$

The coefficients $\mu_{\text{hs},i}^{\text{ex}}$ here are the moment excess chemical potentials of a pure hard sphere system, $\mu_{\text{hs},i}^{\text{ex}} = \partial f_{\text{hs}}^{\text{ex}} / \partial \rho_i$, and also depend only on the ρ_i . The excess part of the free energy (13) of our interacting colloid-polymer mixture thus takes the form

$$f^{\text{ex}} = f_{\text{hs}}^{\text{ex}}(\{\rho_i\}) + \rho_p \sum_i \mu_{\text{hs},i}^{\text{ex}} \sigma_p^i. \quad (15)$$

Recall that in the last term of (15), i.e. in the polymer-colloid interaction, we always use the $\mu_{\text{hs},i}^{\text{ex}}$ derived from the BMCSL free energy.

The excess free energy (15) depends only on a finite number of variables, namely the ρ_i and the polymer density ρ_p . Importantly, these can again be viewed as moments of an *enlarged* density distribution which collects all the densities of our system, namely $(\rho_c(\sigma_c), \rho_p)$. Specifically, we define moments by

$$\rho_i = \int d\sigma_c \rho_c(\sigma_c) w_i^c(\sigma_c) + \rho_p w_i^p \quad (16)$$

in terms of weights ($w_i^c(\sigma_c), w_i^p$) which are made up of a weight function $w_i^c(\sigma_c)$ for the colloid part and a single coefficient w_i^p for the polymer part. The colloidal moment densities, ρ_i , ($i = 0, \dots, 3$) are then given by the weight functions ($\sigma_c^i, 0$) while the polymer density $\rho_p \equiv \rho_4$ is the moment with weight (0, 1).

In summary, our system is described by an excess free energy which depends on five moment densities of the enlarged density distribution $(\rho_c(\sigma_c), \rho_p)$ and is therefore by definition truncatable. This allows us to employ the moment free energy method for the calculation of phase diagrams. As described in [23, 31–33], and for the specific case of polydisperse hard spheres in [2], this maps the full free energy (13), with its dependence on all details

of $(\rho_c(\sigma_c), \rho_p)$ through the ideal part, onto a moment free energy (MFE) $f_{\text{mom}}(\{\rho_i\}) = (\sum_i \lambda_i \rho_i - \rho_{\text{tot}}) + f^{\text{ex}}(\{\rho_i\})$ which depends only on the moments ρ_i ($i = 0, \dots, 4$). Here $\rho_{\text{tot}} = \rho_0 + \rho_4$ is the total number density of colloids and polymers and the λ_i are Lagrange multipliers which depend implicitly on the values of the $\{\rho_i\}$. From this MFE, phase behaviour can then be found by the conventional methods for finite mixtures, treating each of the ρ_i as a number density of an appropriate quasi-species. For truncatable free energies this locates exactly the cloud points, i.e. the onset of phase separation, as well as the properties of the coexisting “shadow” phases that appear there. Inside the coexistence region, one in principle needs to solve a set of highly coupled nonlinear equations and the predictions derived from the MFE are only approximate. However, by retaining extra moments with adaptively chosen weight functions, increasingly accurate solutions can be obtained by iteration [23, 34]. Using these as initial points, we are then able to find full solutions of the exact – for our model free energy – phase equilibrium equations [35, 36].

We work with dimensionless units in the following. We call the overall colloid density distribution in the system the “parent” colloid distribution, $\rho_c^{(0)}(\sigma_c)$, with overall colloid density $\rho_c^{(0)} = \int d\sigma_c \rho_c^{(0)}(\sigma_c)$. The normalised parent size distribution is $n_c^{(0)}(\sigma_c) = \rho_c^{(0)}(\sigma_c) / \rho_c^{(0)}$; we denote its mean diameter by σ_0 . Lengths are measured in units of σ_0 ; the dimensionless polymer diameter σ_p then coincides with the polymer-to-(mean) colloid size ratio ξ . All densities are referred to the volume of a unit colloid particle, $(\pi/6)\sigma_0^3$.

IV. PHASE DIAGRAM TOPOLOGIES

In this section we will describe our results for the overall phase behaviour of a mixture of polydisperse hard spheres and monodisperse polymers. Our numerical work requires a choice to be made for the colloidal parental diameter distribution. We focus on a triangular distribution,

$$n_c^{(0)}(\sigma_c) = \frac{1}{w^2} \begin{cases} \sigma - (1 - w) & \text{for } 1 - w \leq \sigma_c \leq 1 \\ (1 + w) - \sigma & \text{for } 1 \leq \sigma_c \leq 1 + w \end{cases}$$

whose width parameter w is related to the polydispersity by $w = \sqrt{6} \delta$. For the moderate values of δ of interest here one expects other distribution shapes to give qualitatively similar results. As in the case of polydisperse hard spheres without added polymer, this is based on the intuition that for narrow size distributions δ is the key parameter controlling the phase behaviour [1, 2, 37].

To assess the range of possible phase diagram topologies we consider initially four combinations resulting from having either small or large polymers, $\xi = 0.2$ and 0.4 , and colloids with small or moderate polydispersity, $\delta = 0.05$ and 0.08 . Fig. 2 shows the resulting phase diagrams in the $\phi_c - \phi_p$ plane. The nature of the different

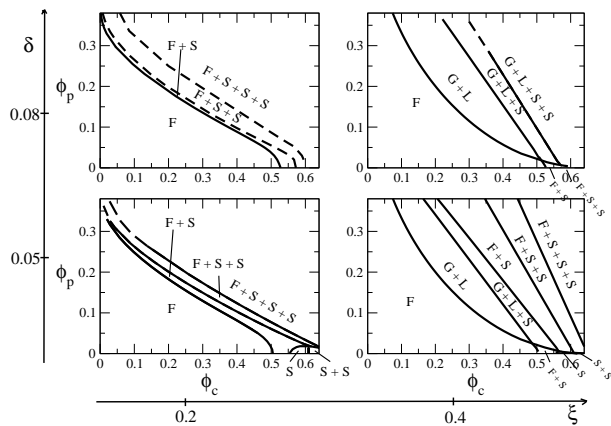


FIG. 2: Phase diagram on a 2×2 grid of values of $(\xi, \delta) \in \{0.2, 0.4\} \times \{0.05, 0.08\}$. In each region the nature of the phase(s) coexisting at equilibrium is indicated (F: fluid, S: solid, G: gas, L: liquid). The dashed lines indicate the best guess of the phase boundary in regions where our numerical data become unreliable.

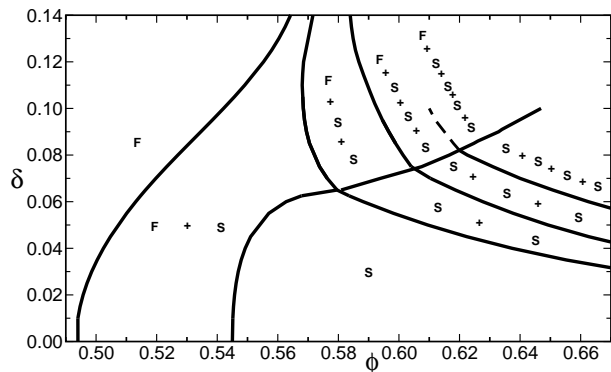


FIG. 3: Phase diagram for polydisperse hard spheres without added polymer. Note the appearance of regions with multiple solid coexistence as polydispersity increases. Horizontal cuts at $\delta = 0.05$ and 0.08 give the behaviour along the baselines of the graphs in the previous figure. From [1].

coexisting phases, i.e. gas, liquid, fluid and solid, is indicated in each region. Probably the most striking feature of these phase diagrams is the presence of multiple solids: in addition to the phases that are found for monodisperse colloids (see Fig. 1), size polydispersity in the colloids allows the system to phase separate into several solid phases.

Qualitatively, the phase diagrams of Fig. 2 can be understood by combining the behaviour observed in two simpler cases: the limit of a mixture of polymers and *monodisperse* colloids, which gives the phase diagrams sketched in Fig. 1, and the polymer-free limit of polydisperse hard-sphere colloids [1, 2], with phase diagram shown in Fig. 3. The first limit clarifies why we need to distinguish between small and large polymer sizes: the short- or long-range nature of the depletion interaction

dictates whether or not gas-liquid phase separation occurs. The second case of pure colloids clarifies the role of polydispersity in the phase behaviour. In fact the baseline ($\phi_p = 0$) of each diagram in Fig. 2 corresponds to a horizontal cut at the appropriate colloid polydispersity δ in the polymer-free phase diagram of Fig. 3. The multiple solid phases occurring in Fig. 2 are thus “inherited” from the phase behaviour of the polydisperse colloid system without polymer.

Having explained the broad intuition behind Fig. 2, let us look at the individual phase diagrams in more detail. Consider first the case with small polymers, $\xi = 0.2$, and moderate colloid polydispersity, $\delta = 0.05$. From Fig. 3 we see that as we move along a dilution line at $\delta = 0.05$, i.e. as we increase the colloid density at fixed normalised parent size distribution, we have the following sequence of phase splits: $F \rightarrow F+S \rightarrow S \rightarrow S+S \rightarrow \dots$. This sequence re-occurs on the baseline of the bottom left graph of Fig. 2 as it must. If we now gradually add polymers to the solution we find that, as in the monodisperse case, the $F+S$ coexistence region becomes wider; but in the polydisperse case, the boundary between the $F+S$ and S regions eventually meets that between the S and $S+S$ regions, resulting in a triple point that marks the beginning of an $F+S+S$ coexistence region. A phase split of this type is not present in the polymer-free system at this polydispersity δ and results from the interplay of the polymer-generated attraction force, which favours fluid-solid phase splits over single-phase solids, and the polydispersity of the colloids. At higher values of polymer or colloid concentration, coexistence of a fluid with an increasing number of solids then occurs.

At higher colloid polydispersity, $\delta = 0.08$, the phase diagram topology is different. On the $\phi_p = 0$ baseline the phase split sequence now consists of a fluid phase coexisting with an increasing number of solid phases, at least up to $\phi_c \approx 0.63$. As Fig. 2 (top left) shows, all these phase boundaries are affected by the addition of polymer in the same way as the boundary between F and $F+S$ in the monodisperse case, shifting to smaller ϕ_c as ϕ_p is increased. There are no phase boundaries at which a fluid phase is lost and which would move to *larger* ϕ_c , as was the case for the $F+S \rightarrow S$ boundary at $\delta = 0.05$. Consequently no phase boundaries meet with increasing ϕ_p and the phase split sequence remains as for the polymer-free system.

Using similar arguments it is possible to explain the topologies at $\xi > \xi_c$. In the system with polydispersity $\delta = 0.05$ shown in Fig. 2 (bottom right), we see again that the polymer-induced attraction favours fluid-solid splits. As the polymer concentration is increased from the baseline – which is the same as in Fig. 2 (bottom left) – the phase equilibria therefore acquire an additional fluid phase, via transitions from F to $G+L$, from $F+S$ to $G+L+S$ and from S to $F+S$. Because of the colloid polydispersity, however, the same mechanism now also causes coexistence of a fluid with several solids, with e.g. $S+S$ becoming $F+S+S$. At higher level of polydispersities

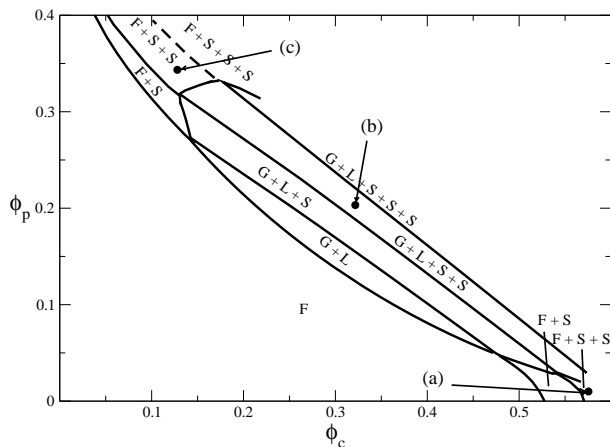


FIG. 4: Phase diagram at $\xi = 0.3$ and $\delta = 0.08$. Note the topology at high polymer concentrations where the region of gas-liquid phase splits terminates, giving way to phase separation involving only a single fluid phase and one or more solids. The arrows indicate at which points in the phase diagram the diameter distributions in Fig. 13 below are calculated.

($\delta = 0.08$, Fig. 2 (top right)), all phase splits on the baseline already contain a fluid phase which splits into G+L on adding polymer. In particular, this mechanism turns F+S+S into G+L+S+S, a polydispersity-induced coexistence of gas, liquid, and two solids.

What remains unclear in this last phase diagram (Fig. 2 (top right)) is how the phase boundaries meet at high polymer concentration. In order to understand this we explored an intermediate polymer size $\xi = 0.3$ at the same polydispersity $\delta = 0.08$. This is easier computationally than exploring higher polymer densities at $\xi = 0.4$ because the smaller value of $\xi = 0.3$ moves the interesting region of the phase diagram to lower ϕ_p . As Fig. 4 demonstrates, the region involving gas-liquid separation eventually terminates at high density, forming a closed “loop”; above this loop one has a single fluid phase coexisting with one or multiple solid phases.

The phase diagram topologies that we have shown so far are the most common that we have encountered, but are not the only ones possible. This is clear from two arguments. First, we have not exhausted all possible sequences of phase splits along the polymer-free baseline; for colloid polydispersity $\delta = 0.07$, for example, Fig. 3 shows that the sequence is $F \rightarrow F+S \rightarrow F+S+S \rightarrow S+S \rightarrow S+S+S \rightarrow \dots$. Second, at constant colloid size distribution the phase diagrams need to change smoothly as the polymer size ξ is varied, connecting e.g. the phase diagrams on the left of Fig. 2 to those on the right. In Fig. 5 we show a sketch of the various topologies that should result as colloid polydispersity δ and polymer size ξ are varied. The usual rule that exactly one phase must be lost or gained on crossing a boundary and the condition of smooth variation with ξ and δ constrain the possible topologies to a large extent. They do not, however, make them fully unique, and Fig. 5 shows a pos-

sible alternative topology for one of the phase diagrams (middle right). Nevertheless, we believe that the scenario shown in Fig. 5 is the most physically plausible sequence of phase diagram topologies. The topology shown in the top right corresponds to Fig. 4 and the top right of Fig. 2, although the numerically calculated phase diagrams do not extend sufficiently far to see all the different phase splits expected theoretically. The remaining phase diagrams in Fig. 2 correspond similarly to top left and bottom left and right of Fig. 5.

One intriguing feature of the predicted topologies is that phase splits involving gas and liquid phases can persist even after the region of pure G+L phase equilibrium has vanished from the phase diagram. This is visible in the middle and top rows of Fig. 5. As ξ is decreased, the gas-liquid loop retracts relative to the onset of fluid-solid phase separation. At the value of ξ where the two boundaries cross, the area of the G+L-region has shrunk to zero. However, a three-phase G+L+S-region of finite size survives at this point, and cannot disappear discontinuously as ξ is varied. Thus phase equilibria involving gas and liquid phases can occur even if the *initial* phase separation that occurs on increasing density is always into fluid and solid phases. This effect is possible only because of the size polydispersity of the colloids.

V. QUANTITATIVE ANALYSIS OF PHASE DIAGRAMS

So far we have discussed the possible topologies of the phase diagrams of our colloid-polymer mixture. In the present section we will study their quantitative dependence on the colloid polydispersity as well as on the polymer-colloid size ratio ξ . We first analyse the behaviour of the cloud and shadow curves which define the onset of phase coexistence, and consider the dependence of the crossover value ξ_c of the polymer size on colloid polydispersity. Fractionation effects are analysed next, both for fluid-solid and for gas-liquid phase separation. Finally we study the shape of the internal phase boundaries between regions with two or more phases, showing how some general features can be predicted with simple arguments.

A. Cloud and shadow curves

The cloud curve defines the onset of phase separation coming from a single-phase region, while the shadow curve records the properties of the incipient phase at this point. We now ask how these curves are affected quantitatively by colloid polydispersity. Looking back at Fig. 2, it is clear that at fixed ξ any such effects on the *cloud curves* are small. In Fig. 6 we show the cloud curves together with the shadows at $\delta = 0.05$ and $\delta = 0.08$.

Also the shadow curves are seen to be only weakly affected by polydispersity. The dotted lines connect-

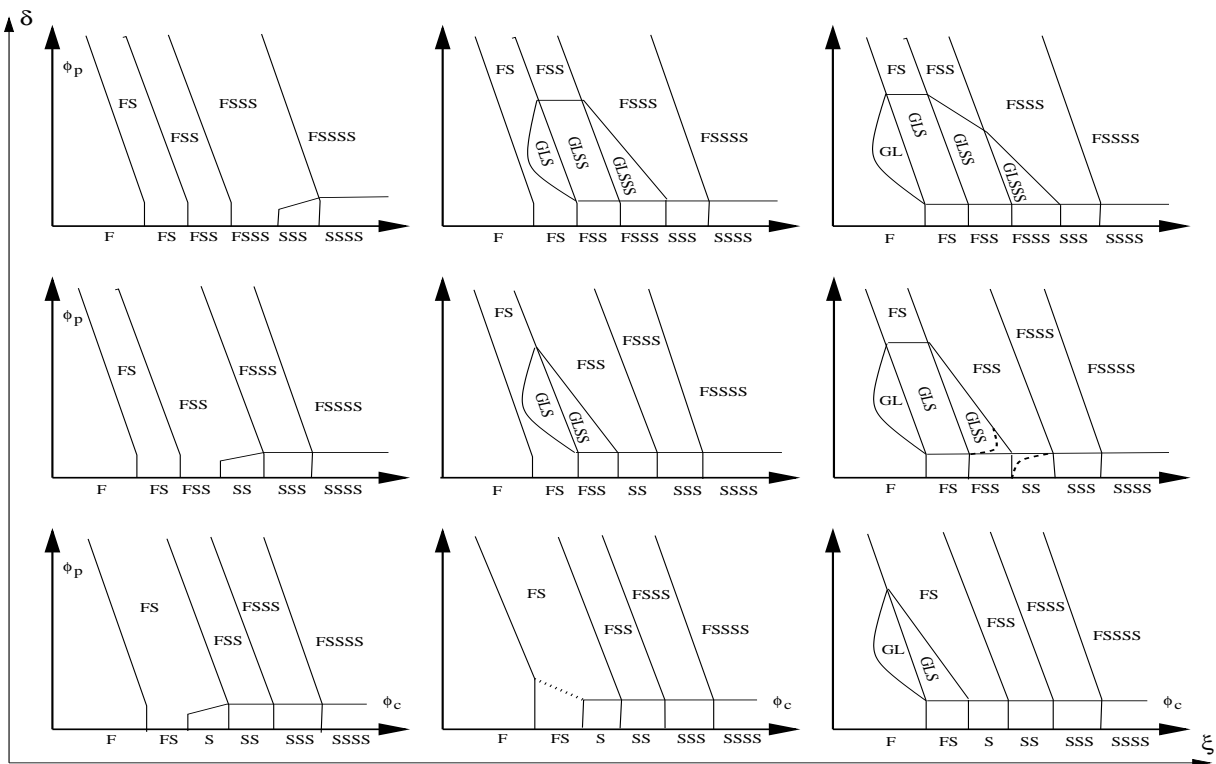


FIG. 5: Sketch of expected phase diagram topologies as a function of polymer size ξ and colloid polydispersity δ . The sequence of phases along the $\phi_p = 0$ -baseline in each row corresponds to $\delta = 0.05, 0.07$ and 0.08 respectively. Middle row, right: Dashed lines indicate a possible alternative topology which can still be connected smoothly to the one below but is physically less plausible. Bottom row, middle: The dotted line indicates the remnant of the G+L+S three-phase region, whose area shrinks to zero at the transition between the two topologies on the left and right.

ing cloud and shadow pairs demonstrate that, as in the monodisperse case, there is strong colloid-polymer fractionation at the onset of phase separation, with the polymer preferably found in the lower-density phase. However, polydispersity does introduce an additional feature, namely colloid size fractionation; this is discussed in the next subsection. We consider next the quantitative effects of polydispersity and polymer size on the onset of gas-liquid phase separation as shown in Fig. 6 (right). To do so, we calculate the location of the gas-liquid critical point and the associated gas-liquid spinodal. These quantities can be obtained in a straightforward way, and without approximation, from the MFE. The conceptual reason for this is that the local stability of a system can be evaluated by only checking the effects of perturbations along the moments contained in the excess part of its free energy [23]. The results are shown in Fig. 7(a) where we plot the previously derived cloud curve at $\xi = 0.4$ and $\delta = 0.05$ together with spinodals and critical points obtained at different values of the polymer size ξ . The dependence on ξ is pronounced. In Fig. 7(b) we contrast this with the change in the location of the critical point as δ rather than ξ is varied. The effect is very much smaller, and would be invisible on the scale of Fig. 7(a). We can nevertheless indicate the *direction* of the shift in

the critical point with increasing δ . This is seen to point inwards, which means that colloid polydispersity tends to delay the onset of gas-liquid separation.

We note briefly that the shift in the critical point coordinates ϕ_c and ϕ_p is quadratic in δ for the modest polydispersities studied here. This arises because the critical point condition only involves moments of the size distribution, all of which are shifted by amounts of $O(\delta^2)$ for small δ . The dependence of the phase boundaries on ξ , on the other hand, is essentially identical to that observed for monodisperse colloids. The spinodals – and, by inference, the cloud curves – shift to the right as ξ decreases; eventually, at the threshold value $\xi = \xi_c$, the G+L phase separation then becomes metastable with respect to the F+S transition.

As reviewed in Sec. I, a number of studies have attempted to locate this threshold value ξ_c of the polymer size, leading to estimates of $\approx 0.3 \dots 0.6$ in theoretical work and ≈ 0.25 in experiments. The effect of colloid polydispersity on ξ_c has remained unclear, however. To address this point, we have investigated different pairs of values for (ξ, δ) and determined the cloud curve for each of them. This is computationally nontrivial because the equilibrium equations need to be solved very accurately to determine the point at which a fluid-solid

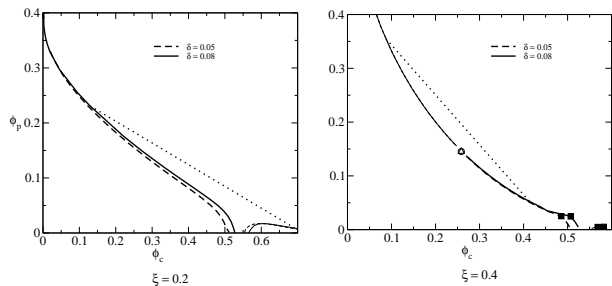


FIG. 6: Plots of cloud (thick line) and shadow (thin line) curves at $\delta = 0.05$ and 0.08 . Dotted lines connect example cloud-shadow pairs. Left: small polymers, $\xi = 0.2$; here the cloud curve marks the onset of fluid-solid phase separation. Right: large polymers, $\xi = 0.4$. The cloud curve at the larger ϕ_p gives the onset of gas-liquid separation. Because cloud and shadow curves at either side of the critical point (marked by the circle and triangle) are almost indistinguishable, we plot only the cloud curve below the critical point and the corresponding shadow above it. At low ϕ_p one has onset of fluid-solid coexistence; the squares mark the triple points where the two branches of the cloud curve meet.

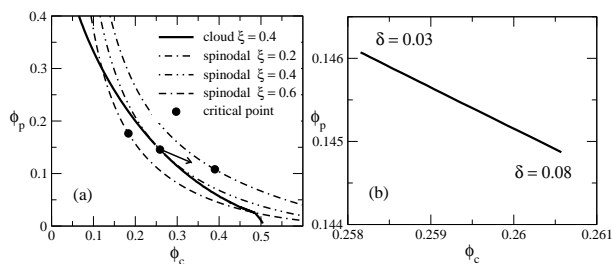


FIG. 7: (a) Spinodal curves obtained for different values of ξ together with the cloud curve at ($\xi = 0.4, \delta = 0.05$) and critical point. (b) Change in the position of the critical point with colloid polydispersity δ , at fixed polymer size $\xi = 0.4$.

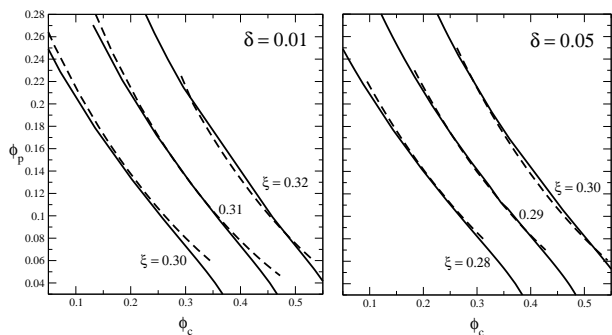


FIG. 8: Plot of the phase boundaries defining the onset of F+S (solid line) and G+L (dashed line) coexistence, at colloid polydispersities $\delta = 0.01$ (left) and $\delta = 0.05$ (right). To make the curves at different polymer sizes ξ visually distinguishable, those for the lowest and highest ξ -values have been shifted along the horizontal ϕ_c -axis by -0.1 and 0.1 respectively.

binodal in a polydisperse system interchanges stability with a gas-liquid binodal. Fig. 8 summarises our results for two different colloid polydispersities. For $\delta = 0.01$, we see that the gas-liquid binodal becomes unstable at $\xi_c = 0.31 \pm 0.01$, while at $\delta = 0.05$ this is shifted to the lower value $\xi_c = 0.29 \pm 0.01$. We see that polydispersity *favours* gas-liquid over fluid-solid phase separation, shifting the threshold polymer size above which stable gas-liquid phase coexistence is observed to lower values. Indeed, for a system with larger colloid polydispersity ($\delta = 0.1$, data not shown) we find a further significant shift to $\xi_c = 0.25 \pm 0.01$. This is in good agreement with the experimental data [5] – though for a somewhat larger polydispersity than quoted in [5] – and is significantly below the value $\xi_c = 0.32$ found in [10] for monodisperse colloids. In summary, colloid polydispersity has significant effects on the threshold value ξ_c for the polymer size, with a δ of only 10% reducing it from $\xi_c \approx 0.31$ to $\xi_c \approx 0.25$.

Several further comments are in order. First, for small δ one would expect ξ_c to be decreased from its monodisperse value by terms of order δ^2 . This is because phase boundaries should generically shift by terms of this order [21, 22] as polydispersity is increased, while they should react smoothly, i.e. linearly, to changes in ξ . Unfortunately, we do not have at present sufficient (and sufficiently precise) data to verify this expectation. Second, our predicted $\xi_c = 0.31$ for $\delta = 0.01$ is just slightly smaller than the monodisperse value $\xi_c = 0.32$ from [10]. This could be due to the small polydispersity in our case, though if shifts in ξ_c are indeed of order δ^2 then $\delta = 0.01$ should give a shift 100 times smaller than that ($0.31 - 0.25 = 0.06$) observed for $\delta = 0.1$, which would be negligible. More likely the small difference is due to the fact that in [10] the scaled-particle or Percus-Yevick expression was used for the free volume term $\mu_{hs}^{ex}(\sigma_p)$ in (13) while we employ the BMCSL expression, consistently with the free energy f_{hs}^{ex} describing the colloidal fluid. Finally, we recall from Sec. V A that colloid polydispersity *delays* the onset of gas-liquid coexistence. On the other hand, we just saw that it *favours* gas-liquid separation *relative* to fluid-solid. The conclusion is that polydispersity must disfavour fluid-solid coexistence, and do so more strongly than for gas-liquid. This is quite plausible, since polydispersity causes inefficient particle packing in a crystalline structure, while it can actually increase packing efficiency in a liquid.

B. Fractionation effects

As pointed out above, in colloid-polymer mixtures with polydisperse colloids the onset of phase separation causes fractionation not just between the colloids and the polymer, but also between the various sizes of colloid particles. To demonstrate this, Fig. 9 (left) shows how the polydispersities of the fluid and solid phases vary along the cloud and shadow curves of Fig. 6 (left). On the x -

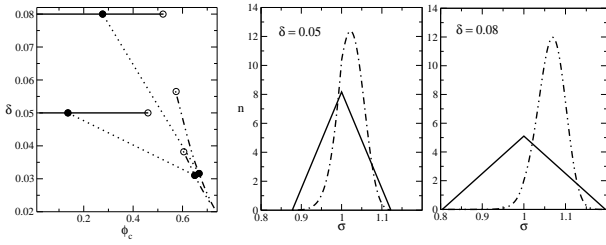


FIG. 9: Left: Polydispersity δ of the fluid cloud and solid shadow phases versus their colloid volume fraction ϕ_c , at the onset of F+S coexistence for $\xi = 0.2$ and parent polydispersity 0.05 and 0.08. See Fig. 6 (left) for the corresponding polymer volume fractions ϕ_p . Solid lines refer to the fluid cloud phase, dot-dashed lines to the solid shadow; dotted lines connect sample cloud-shadow pairs. Middle and right: Example plots of the normalised colloid size distributions of the phases indicated by the circles in the left plot.

axis we plot the colloid volume fraction ϕ_c of the phases, so that the phases are now represented in terms of (ϕ_c, δ) instead of (ϕ_c, ϕ_p) as before. The corresponding values of ϕ_p can of course be read off from the cloud and shadow curves in Fig. 6 (left). In particular, the ends of the lines in Fig. 9 (left), marked by empty circles, correspond to the limit $\phi_p \rightarrow 0$. Examples of the normalised colloid size distributions, $n_c(\sigma_c) = \rho_c(\sigma_c) / \int d\sigma_c \rho_c(\sigma_c)$, are shown in Fig. 9 (middle and right). These results give a concrete demonstration of the fact that the depletion interaction can be used to systematically control and reduce the polydispersity of colloidal mixtures, as has been known for a number of years. In particular Bibette [38] suggested a procedure where colloid samples are fractionated from solutions of volume fraction $\phi_c \approx 0.1$. As we can see from Fig. 9 (left), this is indeed the regime where fractionation is strongest, i.e. where the shadow phase has a much smaller polydispersity than the parent (which is identical to the cloud phase). For phase separation at larger ϕ_c , corresponding from Fig. 6 (left) to smaller polymer volume fractions ϕ_p , the reduction in polydispersity is less pronounced.

Colloidal size fractionation effects do of course occur not only in fluid-solid phase separation, but also in gas-liquid coexistence. Evans *et al* [21, 22] used a perturbative approach to study such fractionation effects for near-monodisperse parent size distributions. They predicted that the difference in mean particle diameters of two coexisting phases, $\Delta\bar{\sigma}_c = \bar{\sigma}_c^{(1)} - \bar{\sigma}_c^{(2)}$, should universally scale as δ^η for small δ , with exponent $\eta = 2$. In [9] Fairhurst and Evans verified this relation experimentally for a colloid-polymer mixture: they used solutions of colloidal PMMA with random polystyrene coils, with size ratio $\xi = 0.45$. Collecting data from a number of samples with parental colloid and polymer volume fractions in the region $\phi_c = 0.15 \dots 0.5$ and $\phi_p = 0.15 \dots 0.3$, they estimated a power-law exponent $\eta = 2.16 \pm 0.44$.

To compare our numerical results with these exper-

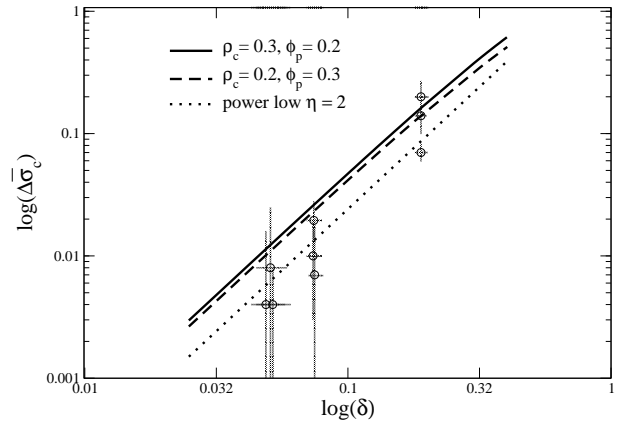


FIG. 10: Log-log plot of the difference in mean colloid diameter between coexisting gas and liquid phases, as a function of the parent polydispersity. The polymer-colloid size ratio is $\xi = 0.45$. Solid and dashed lines show our predictions for two different choices of colloid and polymer concentration, as indicated in the legend. The dotted line is a power law with exponent $\eta = 2$. The circles, together with grey error bars, indicate the experimental data points from [9], which were obtained from a set of samples in the range $\phi_c = 0.15 \dots 0.5$, $\phi_p = 0.15 \dots 0.3$.

imental data, we considered the same polymer-colloid size ratio $\xi = 0.45$ and two different choices for colloid and polymer concentrations, $(\rho_c = 0.3, \phi_p = 0.2)$ and $(\rho_c = 0.2, \phi_p = 0.3)$, with colloid polydispersity ranging from $\delta = 0.025$ to 0.40. We fix ρ_c rather than ϕ_c here since this is the case considered in the perturbative theory. The colloid volume fraction $\phi_c = \langle \sigma_c^3 \rangle \rho_c$ then increases with δ and lies between 0.2 (for $\rho_c = 0.2$ and small δ) and 0.45 (for $\rho_c = 0.3$ and the largest δ). The overall range of variation of ϕ_c and ϕ_p is thus comparable to but somewhat smaller than in the experiments of [9]. Fig. 10 shows our numerical predictions for the difference in mean diameter of the coexisting gas and liquid as a function of parent polydispersity, together with the data from [9]. As expected our calculations are consistent with the universal quadratic scaling at small polydispersities. More importantly, they also show reasonable quantitative agreement with the experimentally measured values. More precise experiments covering a narrower range of colloid and polymer concentrations would obviously be useful, to permit a more stringent test of our calculations.

C. Inner phase boundaries

Having discussed the properties of the cloud and shadow curves, and the fractionation effects which occur at or near the onset of phase separation, we now turn to the internal phase boundaries and their dependence on the polydispersity and polymer-colloid size ratio.

A general trend apparent from Fig. 2 is that, with

increasing polymer concentration, the phase boundaries shift systematically to lower colloid volume fraction. Phase separation into several solids, for example, can thus occur at much lower colloid concentration than in a system without polymer. An intuitive explanation for this is that the osmotic pressure in the system is increased as polymers are added. This compresses the colloids and can be viewed as effectively increasing the colloid volume fraction. From Fig. 3, phase equilibria involving several solids will then occur earlier, as we observe.

Quantitatively, perhaps the most striking feature of Fig. 2 (right) is the fact that for large polymers the internal phase boundaries which continue those in the polymer-free system are almost linear in the (ϕ_c, ϕ_p) -plane. For the boundaries of the G+L+S region in Fig. 2 (bottom right) this is straightforward to rationalise. For monodisperse colloids, the colloid-polymer mixture contains only two different particle species and so the boundaries of the three-phase G+L+S triangle must be *exactly* straight; compare Fig. 1. Introducing a small degree of polydispersity δ should then leave these boundaries approximately straight as observed. This explanation already falters for Fig. 2 (top right), however, where the G+L+S region widens rather than narrows as ϕ_p increases, precluding a straightforward analogy with the three-phase triangle in a monodisperse system. It fails completely for the inner phase boundaries marking the transition between phases involving several solids, which are induced purely by polydispersity effects and have no monodisperse analogue. A different explanation is therefore required: we will see that the near-linearity of the inner phase boundaries arises from the fact that the gas phase consists almost entirely of polymers, plus a negligible amount of colloids. It can therefore act as a “polymer buffer” for the other phases, which contain only small amounts of polymer and are otherwise similar to those in the pure colloid system. For concreteness we focus below on a case where these colloid-rich phases are solids, but the argument applies equally well when there is a liquid among them.

To substantiate this hypothesis, we have extracted in Fig. 11 the properties of the coexisting phases for polymer size $\xi = 0.4$ and polydispersity $\delta = 0.05$, along the phase boundary between the F+S+S and F+S+S+S regions highlighted by the bold line in Fig. 11 (a). The position along the boundary in the plots (b-f) is parameterised by the parent polymer volume fraction $\phi_p^{(0)}$, i.e. the y -coordinate from (a). In (d) and (e) we show the polymer and colloid volume fractions in the various phases. We see that, as anticipated, the fluid phase consists almost entirely of polymers, i.e. it is an extremely dilute colloidal gas. The solids, on the other hand, are essentially pure colloid phases and contain almost no polymer. In addition, as plots (e) and (f) show, their properties remain unchanged along the phase boundary and can be inferred from the extrapolation to the polymer-free limit $\phi_p^{(0)} = 0$. This applies in particular to their common pressure Π^* , and the average colloid volume fraction

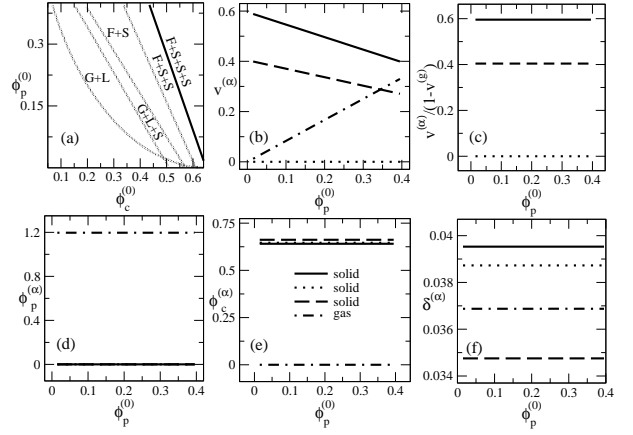


FIG. 11: Properties of the coexisting phases, for a system with $\xi = 0.4$ and $\delta = 0.05$, along the phase boundary shown in (a) by the dark line. (b) Fractions of system volume $v^{(\alpha)}$ occupied by the various phases; the newly forming solid has vanishing fractional volume. (c) Fractional volumes of the solids normalised by the total fractional volume occupied by solid phases. (d,e,f) Polymer and colloid volume fractions and colloid polydispersity of the coexisting phases.

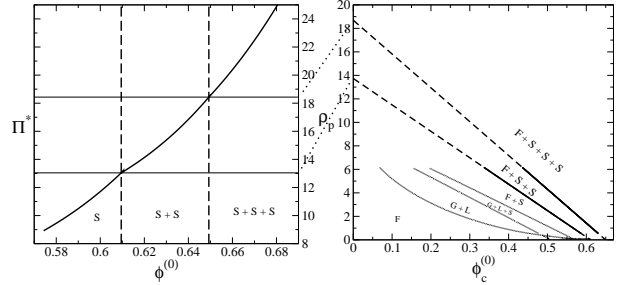


FIG. 12: Left: Pressure plot of a polymer-free system with polydispersity $\delta = 0.05$. The values of the pressure at the phase transitions are marked by the horizontal lines. Right: Phase diagram of a colloid-polymer mixture with the same colloid polydispersity and polymer size $\xi = 0.4$, plotted as $\rho_p^{(0)}$ vs $\phi_c^{(0)}$. Two phase boundaries are extrapolated (dashed) to $\phi_c^{(0)} = 0$. The agreement between the extrapolated values of the intercepts, 13.7 and 18.7, and the equilibrium coexistence pressures Π^* in the polymer-free system, 13.0 and 18.4, is good.

in the solids, ϕ_c^* . The fractional system volumes $v^{(\alpha)}$ occupied by the solids also need to remain in constant proportion to each other, to maintain the overall colloid size distribution, consistent with the results shown in Fig. 11 (b). Figure 11 (c) shows, more explicitly, that when we normalise the fractional volumes of the solid phases by the total fractional volume of all solids, they become constant along the phase boundary. The normalisation factor is $\sum_{\alpha \neq g} v^{(\alpha)} = 1 - v^{(g)}$, where “g” denotes the gas phase.

We can now infer the shape of the phase boundary.

Since only the solid phases contain significant concentrations of colloid, particle number conservation requires that the parental colloid volume fraction is given by

$$\phi_c^{(0)} = (1 - v^{(g)})\phi_c^* \quad (17)$$

Similarly, because the polymers are found almost exclusively in the gas, we have

$$\phi_p^{(0)} = v^{(g)}\phi_p^{(g)} = v^{(g)}\xi^3\rho_p^{(g)} \quad (18)$$

Here we have used the fact that in our density units the polymer density ρ_p and volume fraction ϕ_p are related simply by a factor ξ^3 . In the same units, the pressure of the gas phase is $\Pi^{(g)} = \rho_p^{(g)}$ because the polymers are ideal and the colloids make only a negligible contribution. At equilibrium this pressure must equal that in the colloid phases, Π^* , hence

$$\rho_p^{(g)} = \Pi^* \quad (19)$$

Combining the last three equations now gives the desired relation between the parent polymer and colloid volume fractions along the phase boundary:

$$\rho_p^{(0)} = \xi^{-3}\phi_p^{(0)} = \Pi^* \left(1 - \frac{\phi_c^{(0)}}{\phi_c^*}\right) \quad (20)$$

This is indeed linear, as we set out to show, and obeys the general trend that with increasing $\phi_p^{(0)}$ phase transitions occur at smaller parental colloid volume fractions $\phi_c^{(0)}$. The relation (20) also predicts that if we extrapolate the straight phase boundaries to $\phi_c^{(0)} = 0$, i.e. to their intersection with the y -axis, the intercept will be $\phi_p^{(0)} = \xi^3\Pi^*$, or $\rho_p^{(0)} = \Pi^*$ if we plot $\rho_p^{(0)}$ on the y -axis. In Fig. 12 we check this prediction explicitly for two of the numerically calculated phase boundaries of the system in Fig. 11, finding good agreement. More generally, one concludes from (20) that all the straight phase boundaries in systems with sufficiently large polymers should become approximately independent of the actual polymer size ξ , once they are plotted in terms of $\rho_p^{(0)}$ versus $\phi_c^{(0)}$. The restriction here is that the polymers must not be too close to the threshold size ξ_c . This ensures that the straight phase boundaries extend close to the polymer-free baseline, thus justifying our extrapolation to $\phi_p = 0$ to determine Π^* and ϕ_c^* . For ξ close to ξ_c , on the other hand, as in e.g. Fig. 4 above, the relevant polymer-free “reference system” can no longer be obtained by straightforward linear extrapolation. Nevertheless, our arguments show that along straight internal phase boundaries, and indeed along appropriate straight lines *between* the phase boundaries, the colloidal size distribution of the dense phases should remain approximately unchanged.

To illustrate this phenomenon, we plot in Fig. 13 three examples of normalised colloid diameter distributions at the three points marked in the phase diagram of Fig. 4. These points lie approximately on a straight line following the direction of the phase boundaries. As expected, we find that the size distributions in the liquid

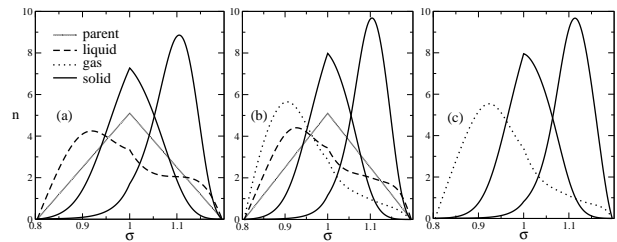


FIG. 13: Normalised colloidal size distributions $n_c(\sigma_c)$ in co-existing phases; the parent distribution is shown for comparison. The three graphs correspond to the values of (ϕ_c, ϕ_p) indicated in Fig. 4.

and solid phases remain approximately constant. This seems rather remarkable, given that the overall colloid and polymer fractions in the three cases are very different.

VI. CONCLUSION AND OUTLOOK

We have studied theoretically, for the first time, the equilibrium phase behaviour of mixtures of *polydisperse* hard sphere colloids and monodisperse polymers. Our treatment is based on the AO model, which treats the polymers as spherical particles interacting only with the colloids. Within the van der Waals approximation of Lekkerkerker *et al*, the polymer-colloid interaction is determined by the excess chemical potentials of the polydisperse hard sphere system. We have therefore used as input suitable free energy approximations for the colloidal fluid and solid, choosing the BMCSL and Bartlett’s “geometric” free energy, respectively; these were shown in previous work to give quantitatively reliable predictions. Complete phase diagrams, taking full account of fractionation effects, are found exactly – to within numerical accuracy – by the use of the moment free energy with extra adaptive moments; this is possible because the free energies involved are truncatable. The intricate features of phase separation in pure polydisperse colloids, including fractionation into several solids, combine with the appearance of polymer-induced gas-liquid coexistence to give a rich variety of phase diagram topologies.

We studied in some detail the dependence of these phase diagrams on colloid size polydispersity δ and the polymer-colloid size ratio ξ . Even for the moderate values of δ we consider ($\delta \leq 0.10$), polydispersity has a significant influence on the number of phases and the topology of the phase boundaries. This influence arises because the sequence of phase transitions that is observed in a “baseline” system of pure colloids changes significantly with δ . Starting from this baseline the addition of polymer then causes fluid phases to phase separate into colloidal gas and liquid, or a new fluid phase to appear if only solids were present in the polymer-free baseline system. The strength of this effect grows with polymer size ξ ; this is

reasonable because both the range and strength of the effective colloid-colloid interaction caused by the presence of polymer grows with ξ . The strength of this attraction also grows with polymer concentration, and consequently all phase boundaries shift to lower colloid concentrations when more polymer is added. In particular, we predict that phase splits involving two or more fractionated solids should occur at fairly moderate colloid volume fractions, where the phase separation kinetics should be substantially faster than for the corresponding higher volume fractions in a system without added polymer. This suggests the exciting possibility that such solid-solid phase splits, which have not hitherto been seen in experiments, may be observable in this regime. We note, however, that the growth kinetics of polydisperse crystals [39] may still cause deviations from the predicted equilibrium behaviour even if the regime of multiple solids is kinetically accessible.

We deduced the possible phase diagram topologies from the requirement that they need to change smoothly with both δ and ξ . One intriguing prediction of this is that, in the presence of colloid polydispersity, stable three-phase gas-liquid-solid coexistence can persist without a corresponding two-phase gas-liquid region in the phase diagram; see the middle and top rows of Fig. 5. This effect should also be observable experimentally, for values of ξ just below the threshold ξ_c at which the stable gas-liquid coexistence disappears.

In our quantitative analysis of the phase behaviour, we found that this threshold value ξ_c depends significantly on colloid polydispersity, decreasing from $\xi_c \approx 0.31$ for $\delta = 0.01$ to $\xi_c \approx 0.25$ for $\delta = 0.1$. We saw that polydispersity delays the onset of both gas-liquid and fluid-solid separation, but that the effect is stronger for the latter, causing the observed shifts in ξ_c . We further considered fractionation effects and found that in fluid-solid coexistence these are most marked for high polymer and low colloid concentration, in agreement with experimen-

tal protocols that are used to reduce polydispersity in colloidal systems. Also for gas-liquid coexistence the calculated fractionation effects are in reasonable agreement with the experimental data, and follow the universal fractionation relation in the limit of small polydispersity. Finally, we observed that, for sufficiently large polymer sizes ξ , boundaries between regions of the phase diagram containing two or more phases are close to straight. This is due to the occurrence of a dilute colloidal gas phase which acts effectively as a polymer buffer. We derived from this an estimate of the location and slope of the phase boundaries in terms of the properties of a corresponding polydisperse colloid system without added polymer.

An interesting extension of this research would be to the case where the *polymers* are polydisperse – with a fixed parent density distribution – while the colloids are monodisperse, or even further to the scenario where both colloids and polymers are polydisperse. Work in this direction is in progress. One would also like to assess the effects of polymer non-ideality, for which a number of theoretical approaches have been developed, based on perturbation theory around the θ -point [40], integral equations [41] and effective colloid-colloid interactions derived from simulations of self-avoiding walk (SAW) polymers [42]. The method that fits most naturally into our framework is to add second-order virial terms to account for polymer-polymer interactions, as done in [40]. However, recent simulation studies [43] indicate that the AO model gives quantitatively reasonable results also for *interacting* (monodisperse SAW) polymers up to quite large sizes $\xi < 0.34$. For larger ξ , where significant deviations arise [43], one has to account both for polymer interactions *and* also increasingly for the detailed polymer chain structure. An “AO + second virial” model which only addresses the first effect is therefore unlikely to be useful over a significant range of ξ .

-
- [1] M. Fasolo and P. Sollich, Phys. Rev. Lett. **91**, 068301 (2003).
- [2] M. Fasolo and P. Sollich, (2004), Preprint cond-mat/0405621.
- [3] S. Asakura and F. Oosawa, J. Chem. Phys. **22**, 1255 (1954).
- [4] A. Vrij, Pure Appl. Chem. **48**, 471 (1976).
- [5] S. M. Ilett, A. Orrock, W. C. K. Poon, and P. N. Pusey, Phys. Rev. E **51**, 1344 (1995).
- [6] V. J. Anderson, E. H. A. de Hoog, and H. N. W. Lekkerkerker, Phys. Rev. E **65**, 011403 (2002).
- [7] W. C. K. Poon, J. Phys.: Condens. Matter **14**, R859 (2002).
- [8] R. Tuinier, J. Rieger, and C. G. De Kruif, Adv. Colloid Interface Sci. **103**, 1 (2003).
- [9] D. J. Fairhurst and R. M. L. Evans, Colloid Polym Sci **282**, 766 (2004).
- [10] H. N. W. Lekkerkerker, W. C. K. Poon, P. N. Pusey, A. Stroobants, and P. B. Warren, Europhys. Lett. **20**, 559 (1992).
- [11] M. Dijkstra, J. M. Brader, and R. Evans, J. Phys.: Condens. Matter **11**, 10079 (1999).
- [12] A. P. Gast, W. B. Russel, and C. K. Hall, J. Colloid Interface Sci. **109**, 161 (1986).
- [13] P. N. Pusey and W. Van Meegen, Nature **320**, 340 (1986).
- [14] S. E. Paulin and B. J. Ackerson, Phys. Rev. Lett. **64**, 2663 (1990).
- [15] W. Götze, Aspects of structural glass transitions, in *Liquids, freezing and glass transition*, edited by J. P. Hansen, D. Levesque, and J. Zinn-Justin, pages 287–503, Amsterdam, 1991, North-Holland.
- [16] A. A. Louis, Philos. Trans. R. Soc. Lond. Ser. A-Math. Phys. Eng. Sci. **359**, 939 (2001).
- [17] P. B. Warren, Langmuir **13**, 4588 (1997).
- [18] R. P. Sear and D. Frenkel, Phys. Rev. E **55**, 1677 (1997).
- [19] J. T. Lee and M. Robert, Phys. Rev. E **60**, 7198 (1999).

- [20] A. R. Denton and M. Schmidt, *J. Phys.: Condens. Matter* **14**, 12051 (2002).
- [21] R. M. L. Evans, D. J. Fairhurst, and W. C. K. Poon, *Phys. Rev. Lett.* **81**, 1326 (1998).
- [22] R. M. L. Evans, *J. Chem. Phys.* **114**, 1915 (2001).
- [23] P. Sollich, P. B. Warren, and M. E. Cates, *Adv. Chem. Phys.* **116**, 265 (2001).
- [24] B. Widom, *J. Chem. Phys.* **39**, 2808 (1963).
- [25] J. J. Salacuse and G. Stell, *J. Chem. Phys.* **77**, 3714 (1982).
- [26] T. Boublik, *J. Chem. Phys.* **53**, 471 (1970).
- [27] G. A. Mansoori, N. F. Carnahan, K. E. Starling, and T. W. Leland, Jr., *J. Chem. Phys.* **54**, 1523 (1971).
- [28] P. Bartlett, *Mol. Phys.* **97**, 685 (1999).
- [29] P. Bartlett, *J. Chem. Phys.* **107**, 188 (1997).
- [30] A. Moncho-Jorda, A. A. Louis, P. G. Bolhuis, and R. Roth, *J. Phys.: Condens. Matter* **15**, S3429 (2003).
- [31] P. B. Warren, *Phys. Rev. Lett.* **80**, 1369 (1998).
- [32] P. Sollich and M. E. Cates, *Phys. Rev. Lett.* **80**, 1365 (1998).
- [33] P. Sollich, *J. Phys.: Condens. Matter* **14**, R79 (2002).
- [34] N. Clarke, J. A. Cuesta, R. Sear, P. Sollich, and A. Speranza, *J. Chem. Phys.* **113**, 5817 (2000).
- [35] A. Speranza and P. Sollich, *J. Chem. Phys.* **117**, 5421 (2002).
- [36] A. Speranza and P. Sollich, *J. Chem. Phys.* **118**, 5213 (2003).
- [37] P. N. Pusey, *J. Phys. (Paris)* **48**, 709 (1987).
- [38] J. Bibette, *J. Coll. Interf. Sci.* **147**, 474 (1991).
- [39] R. M. L. Evans and C. B. Holmes, *Phys. Rev. E* **64**, 011404 (2001).
- [40] P. B. Warren, S. M. Ilett, and W. C. K. Poon, *Phys. Rev. E* **52**, 5205 (1995).
- [41] D. G. A. L. Aarts, R. Tuinier, and H. N. W. Lekkerkerker, *J. Phys.: Condens. Matter* **14**, 7551 (2002).
- [42] A. A. Louis, P. G. Bolhuis, E. J. Meijer, and J. P. Hansen, *J. Chem. Phys.* **117**, 1893 (2002).
- [43] P. G. Bolhuis, A. A. Louis, and J. P. Hansen, *Phys. Rev. Lett.* **89**, 128302 (2002).